Light Metals 2014
Edited by: John Grandfield
TMS (The Minerals, Metals & Materials Society), 2014

X-RAY TOMOGRAPHY AND SMALL-ANGLE NEUTRON SCATTERING CHARACTERIZATION OF NANO-COMPOSITES: STATIC AND *IN SITU* EXPERIMENTS

Sofiane Terzi[1], Rémi Daudin[2], Julie Villanova[3], Prakash Srirangam[4], Pierre Lhuissier[2], Luc Salvo[2], Elodie Boller[3], Ralf Schweins[5], Peter Lindner[5], Jean-Jacques Blandin[2], Peter Lee[4], Hartmut Lemmel[5]

[1]European Space Agency, ESTEC, ILL4, 6 rue Jules Horowitz, 38042 Grenoble Cedex, France
[2]SIMaP, UMR CNRS 5266, Grenoble University, GPM2, BP 46; 38402 Saint-Martin d' Heres Cedex, France
[3]ESRF, 156 rue des Martyrs, BP 220, 38043 Grenoble Cedex 9, France
[4]School of Materials - The University of Manchester; Didcot, Oxfordshire, OX11 OFA, United Kingdom
[5]ILL, 6 rue Jules Horowitz, 38042 Grenoble Cedex, France

Keywords: X-ray tomography, Small-Angle Neutron Scattering, Metal Matrix Nano-Composites, Ultrasonic Melt Processing.

Abstract

To meet the future EU challenges of lightweighting and pollution reduction, especially relevant in transportation, it is necessary to develop innovative materials and processing techniques. The addition of reinforcing nanoparticles coupled with melt treatment by external fields (electromagnetic or ultrasonic) was identified as a promising route to improve light alloys properties. The purpose of this study is to present combined results obtained from small-angle neutron scattering and X-ray tomography on Aluminium (6082) and Magnesium (AZ91) nano-composites in static conditions with different reinforcements. We will discuss the morphology, size, and spatial distribution of particles as well as their influence on the solidification microstructure. We will also present some *in situ* experiments using X-ray tomography and Small Angle Neutron Scattering (SANS) carried out to investigate the influence of ultrasonic vibration on the agglomeration and deagglomeration of particles.

Introduction

Metal Matrix Composites have been studied for a long time but have found very few applications as a structural material due to their very low ductility. This was mainly due to the size of the ceramic reinforcers used (always larger than 10 µm otherwise the particles agglomerate) and their quality. Since the beginning of 2000 new elaboration techniques allow to produce composites with very small particles size (less than 1 µm) with a better control of the particle dispersion thanks to intense shearing or the use of ultrasonic field [1-4]. The great advantage of these new composites, abusively called nano-composites since particles are often larger than 50 nm, is that their strength is largely increased with a small amount of reinforcement (typically few %) without too much decrease in ductility. These new composites are thus considered to meet the future EU challenges of lightweighting and pollution reduction, especially relevant in transportation. This is one the main challenges of the ExoMet European project [5]. Despite the new development presented above there have been very few characterization studies and in particular 3D analyses of the spatial distribution of the reinforcers. According to the size of the particles (usually ranging from 20 nm to 500 nm) and the possible agglomeration, there are several techniques that can be implemented to characterize properly the spatial distribution. Non-destructive techniques allowing direct observation such as micro-tomography can be used to characterize the influence of particle addition on the morphology of the primary phase. When the particles are large enough and have a sufficient absorption contrast with the matrix, their presence can be noticed within the microstructure. However, only nano-tomography is able to provide 3D local information on the agglomeration state of particles i.e. how much particles actually compose a particular aggregate seen as one spot in micro-tomography. Nano-tomography does not allow for *in situ* observation as the acquisition time can reach up to 3 hours to obtain a high resolution image. Indirect observation by Small Angle Scattering (SAS), on the other hand, can provide averaged information over a large volume on the agglomeration state of nano-sized particles. The counterpart is that these information are obtained after some assumptions by fitting intensity-q curves and different interpretations are generally possible. In the present study, a combination of these different types of techniques was used to investigate the effect of ultrasound melt treatment on the dispersion of particles in metal matrix nano-composites.

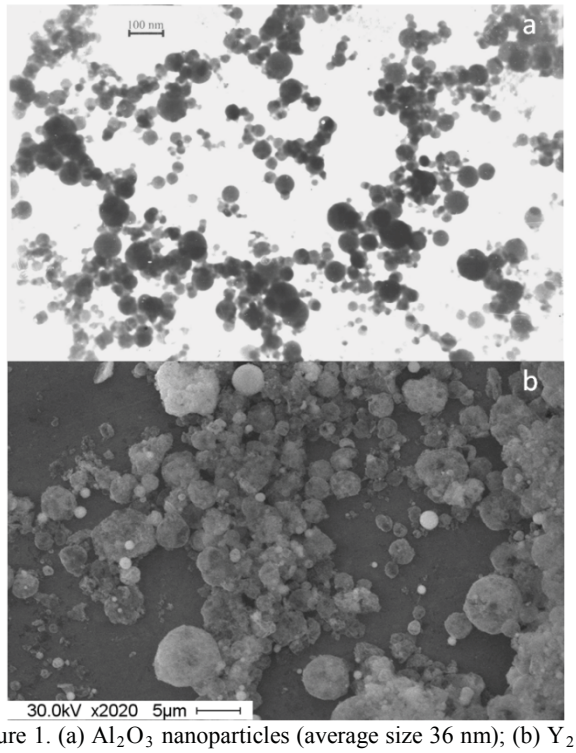

Figure 1. (a) Al_2O_3 nanoparticles (average size 36 nm); (b) Y_2O_3 nanoparticles (average size 500 nm) [5].

Materials And Experimental Procedure

Materials

All materials coming from the EXOMET program and have been produced as described in [5]. Two matrices have been studied in this work: a AZ91 magnesium alloy and a 6082 aluminium alloy and two types of reinforcement have been chosen: Y_2O_3 particles (for the AZ91 alloy) that are approximately 500 nm in size and Al_2O_3 particles (for the 6082 alloy) with a size of approximately 50 nm. SEM images of these two types of ceramic powders are shown in Figure 1a and 1b respectively. Y_2O_3 has been selected since it provides good absorption contrast for X-ray tomography experiments and Al_2O_3 since it gives good scattering contrast for the SANS experiments. Both composites have been produced using ultrasonic treatment before solidification in order to deagglomerate particles. The mass fraction of reinforcement added during processing was the same for both samples (AZ91 reinforced with Y_2O_3 and 6082 reinforced with Al_2O_3) and equal to 1%.

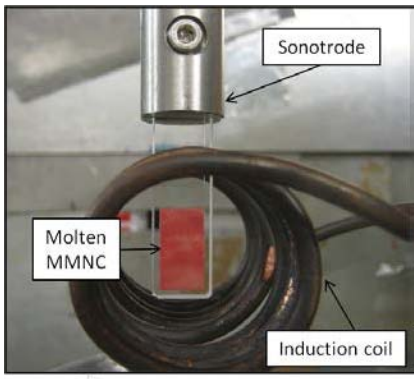

Figure 2. Zoom on the sample holder for the SANS experiments

X-Ray Tomography

X-ray tomography characterization of the AZ91 reinforced with Y_2O_3 has been carried out at the European Synchrotron Radiation Facility (ESRF) on two beamlines ID19 and ID22NI. Room temperature scans have been performed on both lines. Conventional absorption tomography was used on ID19 with a pixel size of 0.55 µm and a CMOS PCODIMAX camera (field of view 1200 x 1200), while holotomography was used on ID22 with a pixel size of 50 nm and with a CCD FreLoN camera (field of view 2048 x 2048). Details on the holotomography set-up and reconstruction can be found elsewhere [6-8]. On ID19 a pink beam of 17.6 KeV was used and 800 projections have been taken over 180°, while an energy of 29.6 keV was used on ID22NI and 2000 projections were taken with an exposure time of 0.5 s. *In situ* remelting experiments have also been conducted on ID19 in order to study the agglomeration of particles in the absence of ultrasonic treatment. The sample (a rod of 1.2 mm in diameter and 3 mm in height) was heated in a furnace developed at ESRF on ID15 with Helium gas and fast tomography acquisition with PCODIMAX during the remelting.

Small Angle Neutron Scattering

Experiments were carried out on D11 at the Institut Laue-Langevin (ILL) on the 6082 reinforced with Al_2O_3 particles. We performed four SANS measurements: (i) a first one on the "as-received" sample (where the particles were ultrasonically dispersed), (ii) a second one on the same material but reheated to the liquid state and without the application of ultrasound, (iii) a third one after solidification of the reheated sample and (iv) a final one after remelting, 10 s of ultrasonic treatment at the liquid state and solidification. The sample (10x15x2 mm rectangular shape) was placed in a quartz cell as shown on Figure 2. An induction furnace (Figure 2) was used to reheat and melt the sample and the temperature was recorded thanks to a calibrated pyrometer.

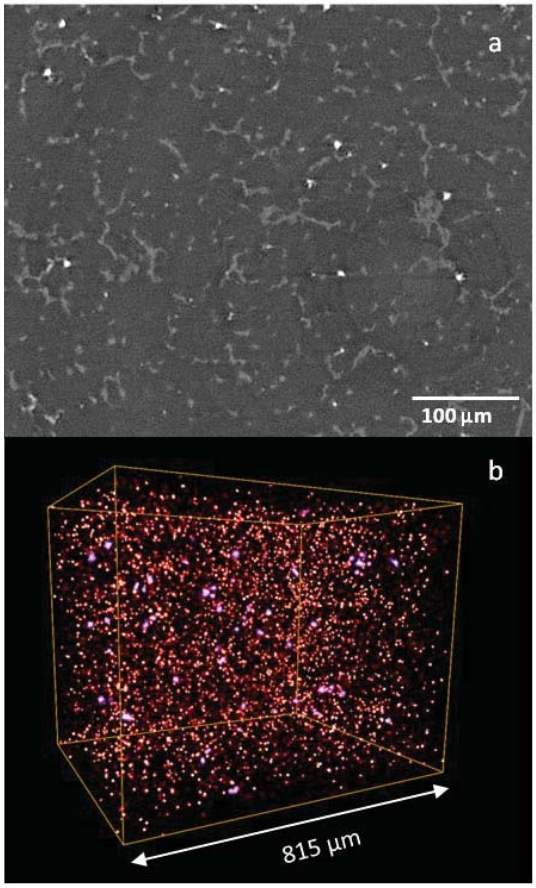

Figure 3. Micro-tomography image of the AZ91/Y_2O_3 composite: (a) extracted slice; (b) 3D rendering.

In order to perform the ultrasonic treatment, the cell was clamped into a sonotrode and 20 kHz vibrations were applied using a piezoelectric transducer and an ultrasonic generator. Two sample-detector distances (8 and 28 m) were used for all investigated states to work in a q range going from 3.0 10^{-3} Å^{-1} to 8.0 10^{-2} Å^{-1} at a neutron wavelength of 6.00 Å. After data treatment that requires the diffusion measurement of an empty cell, deionised water as well as the matrix without particles, the data were reduced and analysed using the formalism of a unified theory developed for systems having different structures on different length scale [9]. Each level is composed of a Guinier and a Porod regime and according to this formalism, the intensity $I_i(q)$ from one level i is given by:

$$I_i(q) = G_i e^{-\frac{q^2 R_{gi}^2}{3}} + e^{-\frac{q^2 R_{g(i-1)}^2}{3}} B_i \left\{ \left(erf\left(\frac{qR_{gi}}{\sqrt{6}}\right)\right)^3 / q \right\}^{P_i} \quad (1)$$

where R_{gi} is the average radius of gyration, G_i a constant relative to the Guinier regime and where B_i and P_i are constants corresponding to the Porod regime of the considered level i.

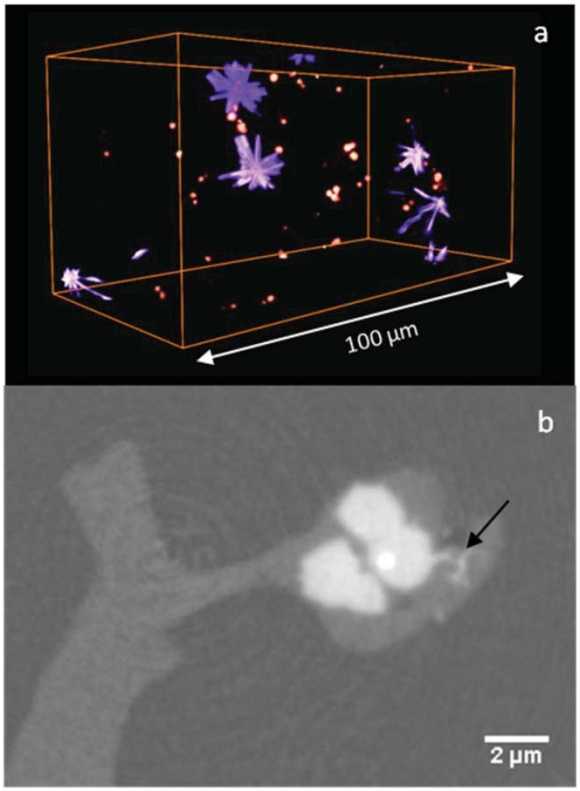

Figure 4. Nano-tomography image of the AZ91/Y_2O_3 composite: (a) 3D rendering of part of the analysed volume, (b) extracted slice. The smaller particles are pointed out by the black arrow.

Results And Discussion

Figure 3a presents a 2D slice obtained from the room temperature tomography of the AZ91/Y_2O_3 composite with a pixel size of 0.55 µm. One can clearly see the primary phase in dark grey, the $Mg_{17}Al_{12}$ phase in light grey and also white spot corresponding to highly absorbent compounds. Some of these spots are most probably the Y_2O_3 particles but considering the low spatial resolution, one cannot determine if these spots consist of one or several particles. Also, they cannot be differentiated from other phases that may form during solidification. Looking at the 2D slices, it can be seen that these white spots are embedded in the $Mg_{17}Al_{12}$ phase meaning that during solidification the Y_2O_3 particles have not been entrapped in the primary phase. The 3D rendering of these white spots (Figure 3b) shows that the spatial distribution is quite good at the scale of the sample since no large aggregate is observed. This is a good indication that the ultrasonic treatment was somehow efficient. The observation of the microstructure has not revealed the presence of large dendrites as usually seen in as cast AZ91 alloys. The primary phase instead is highly tortuous which might be a consequence of the disturbance of the solidification growth front by the presence of particles in the melt [10]. This has probably played a role in the apparent homogeneous spatial distribution of the particles observed after solidification.

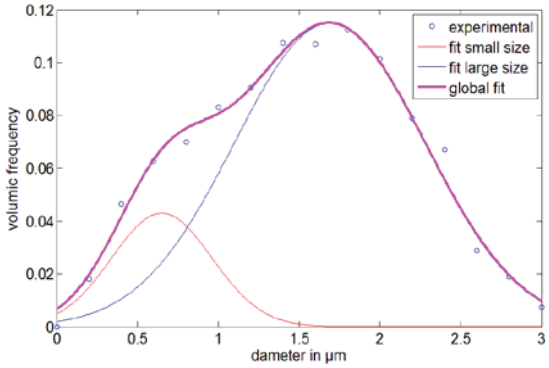

Figure 5. 3D granulometry on equiaxed particles from the 3D data obtained at 50 nm pixel size.

To go deeper in the analysis, X-ray nano-tomography was performed on ID22NI, on the same sample but with much higher spatial resolution (pixel size = 50 nm). The Figure 4a presents a 3D rendering obtained with such imaging conditions. In order to focus on the particles, the primary phase and the $Mg_{17}Al_{12}$ phase were stripped away from the image. From a first sight, two types of particles can clearly be distinguished: equiaxed small particles and highly absorbent star-shaped particles. A closer look to regions where equiaxed particles (Figure 4b) can be found shows that they are structured in small agglomerates of few large (micron-sized) and irregular particles surrounded by smaller (around 500 nm) and more spherical particles. These particles have similar morphology as the Y_2O_3 particles shown in Figure 1b. A 3D granulometry was performed on the 3D volume. The results presented in Figure 5 clearly show a bimodal size distribution which confirms the visual observations. The volume fraction of such particles has been estimated to be about 0.04% meaning that a certain amount of Y_2O_3 particles may have disappeared during solidification. One explanation could be that the star-shaped particles that can be seen on Figure 4a, might come from a reaction between Y_2O_3 particles and the melt explaining this low content of Y_2O_3 particles. These particles appear in bright white and are thus rich in absorbent compounds such as Y. The volume fraction of these particles has been calculated and found to be 0.22%.

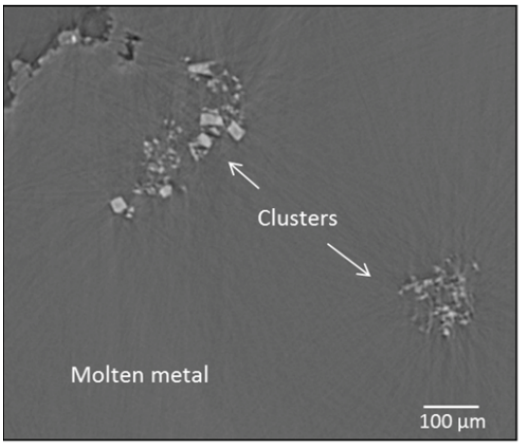

Figure 6. 2D slice of the AZ91/Y2O3 composite in the liquid state after remelting.

The presence of Mn-rich precipitates that are known to form during the solidification of AZ91 alloys has not been clearly identified. Two hypotheses can then be suggested to explain this observation: either the Mn-rich precipitates have similar morphology and absorption properties as the Y_2O_3 particles and some of the equiaxed particles are actually Mn-rich precipitates or some of Mn solute present in the melt has been consumed by the formation of the star-shaped particles. Further chemical analyses (SEM/EDS) are planned to clarify that point. Note that highly spherical particles, with similar absorption properties as the star-shaped particles can be observed inside some of the large and irregular equiaxed particles (Figure 4b). This similarity of absorption property might be an indication of a link between these particles and the star-shaped particles. The AZ91/Y_2O_3 composite have then be remelted and imaged on ID19 once fully liquid. One can observe very rapidly agglomeration of the particles as shown on Figure 6 in 2D and on Figure 7 in 3D rendering. This clearly indicates that treatments, such as ultrasonic processing, are mandatory to deagglomerate particles even if their size is relatively large.

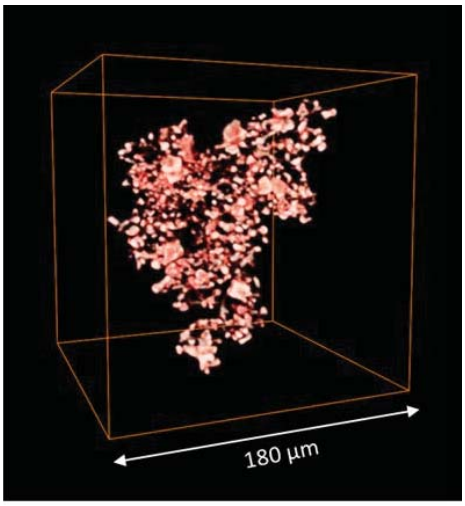

Figure 7. 3D rendering of one of the two large clusters observed in Figure 6.

Concerning the *in situ* SANS experiment on the 6082/Al2O3 composite, two levels were used to fit the results. The first level corresponding to high q, provides information on the individual particles while the second level, corresponding to lower q, gives information on the agglomeration conditions of the particles. The fitted curves are shown in Figure 8. For all states the radius of gyration of individual particles R_{g1} was found to be about 25 nm (Table I). The Porod exponent P_1 was also found to be similar and close to 4 for all states. Such value, i.e. $P = 4$, is predicted for spherical particles. In that case, the average radius of particles R can be calculated using the following formula:

$$R = \sqrt{5/3} R_{g1} \qquad (2)$$

The value found, $R \approx 30$ nm, is in agreement with the order of magnitude specified by the powder manufacturer. For the measurement performed at the liquid state and at the solidified state without ultrasound, fits where only the Porod part of the second level is visible were found to be compatible with the results. In that case, the radius of gyration is too large to be measured from the investigated q range which could be in agreement with the presence of very large agglomerates. For the "as-received" and final state, however, a radius of gyration was calculated and found to be about 70 nm for the first one and about 100 nm for the later one. Value ranging between 2.0 and 2.6 were determined for the Porod exponent of the second levels. This is in agreement with the mass-fractal property of aggregates.

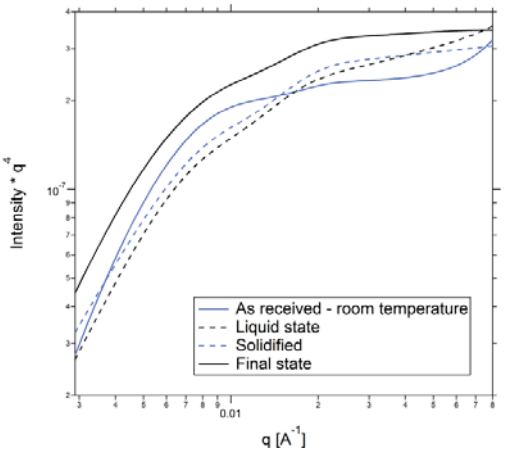

Figure 8. Results of the *in situ* SANS experiment: intensity*q^4 vs q fitted curves for the four investigated states.

Table I. Values found by fitting the results with the unified fit

	R_{g1}	R_{g2}	P_1	P_2
	Å	Å		
As-received	251.4	705.1	3.976	2.575
Liq. state	256.6	NaN	3.764	2.044
Solidified	235.6	NaN	3.896	2.202
Final state	243.3	1008	3.935	2.435

These results are thus compatible with the following scenario: (i) at the beginning of the experiment, the particles are well dispersed in the "as-received" material, (ii) then agglomeration occurs during melting and large clusters are present within the melt, (iii) the solidification that follows does not seem to significantly change the spatial distribution of the Al_2O_3 particles and finally (iv) when the composite is remelted and processed by ultrasounds, a particle dispersion comparable to the one found at initial state is recovered after solidification. This is in agreement with the formation of the large Y_2O_3 particle clusters observed during the *in situ* melting experiment performed on the ID19 micro-tomography beamline.

Conclusion

Different types of characterization techniques were used to investigate the effect of ultrasonic melt treatment on the particle dispersion in molten metal matrix composites. This work presents the first *in situ* melt processing experiment on metallic alloys performed on a beamline. It was found that particle agglomeration occurs readily when materials are remelted. The large particle clusters that form in the melt then remain in the solidified microstructure. The results show that particle dispersion by ultrasonic processing seems to be an efficient way to avoid the formation of such large agglomerates. Further investigations using different imaging techniques are planned to correlate the SANS results obtained on the Al_2O_3 nano-composite with direct observations.

References

[1] S. Lakshmi, et al., *In situ preparation of TiB2 reinforced Al based composites*, J. Mater. Process. Technol., 73 (1998) 160-166.
[2] H. Su, et al., *Processing, microstructure and tensile properties of nano-sized Al2O3 particle reinforced aluminum matrix composites*, Materials & Design, 36 (2012) 590-596.
[3] C.S. Ramesh, et al., *Development of Al 6063–TiB2 in situ composites*, Materials & Design, 31 (2010) 2230-2236.
[4] S.S.S. Kumari, et al., *Synthesis and characterization of in situ Al–AlN composite by nitrogen gas bubbling method*, J. Alloys Compd., 509 (2011) 2503-2509.
[5] W.H. Sillekens, et al., *The ExoMet Project: EU/ESA Research on High Performance Light Metal Alloys and Nanocomposites*, Submitted to Metallurgical and Materials Transactions A.
[6] G. Martinez-Criado, et al., *Status of the hard X-ray microprobe beamline ID22 of the European Synchrotron Radiation Facility*, Journal of Synchrotron Radiation, 19 (2012) 10-18.
[7] P. Cloetens, et al., *Holotomography: Quantitative phase tomography with micrometer resolution using hard synchrotron radiation x rays*, Appl. Phys. Lett., 75 (1999) 2912-2914.
[8] V. Julie, et al., *3D phase mapping of solid oxide fuel cell YSZ/Ni cermet at the nanoscale by holographic X-ray nanotomography*, J. Power Sources, 243 (2013) 841-849.
[9] G. Beaucage, *Approximations Leading to a Unified Exponential/Power-Law Approach to Small-Angle Scattering*, J. Appl. Crystallogr., 28 (1995) 717-728.
[10] L. Granasy, et al., *Growth of 'dizzy dendrites' in a random field of foreign particles*, Nat Mater, 2 (2003) 92-96.

Acknowledgements

The authors wish to acknowledge financial support from the ExoMet Project, which is co-funded by the European Commission in the 7th Framework Programme (contract FP7-NMP3-LA-2012-280421), by the European Space Agency and by the individual partner organisations. Helmholtz-Zentrum Geesthacht and Brunel University are also acknowledged for providing the composite materials used in this study.